Computational Studies Exploring the Relationship between Flame Lift-Off Height and Soot Formation in Diesel Jets

May Yen[1,*] John Abraham[1,2]
[1]School of Mechanical Engineering, Purdue University, West Lafayette, IN 47907-2088, USA
[2]School of Mechanical Engineering, University of Adelaide, Adelaide, South Australia 5005, Australia

Abstract

It has been suggested that fuel/air mixing upstream of the lift-off height influences the formation of soot in reacting diesel jets. Hence, greater lift-off height results in more mixing, resulting in less soot. In this work, computations of reacting diesel jets are carried out for a wide range of conditions by employing a RANS model in which an unsteady flamelet progress variable (UFPV) submodel is employed to represent turbulence/chemistry interactions. The conditions selected reflect changes in injection pressure, chamber temperature, oxygen concentration, ambient density, and orifice diameter. As reported in prior work, the UFPV model predicts the ignition delay and flame lift-off height within about 25% of reported measurements. Soot is modeled using a kinetic model in which hydrogen-abstraction followed by carbon-addition results in the formation of polycyclic aromatic hydrocarbons (PAHs) which act as precursors to soot. For all cases, except the cases with different orifice diameter and ambient density, the soot concentration decreases with increasing lift-off height when the lift-off height is appropriately normalized. Analysis of the entrained mass upstream of the lift-off height confirms that this correlation arises from variation in entrained mass.

Keywords: diesel, jets, lift-off height, soot, formation

1. Introduction

Understanding soot formation in reacting diesel jets as it relates to lift-off height L_f is important as the behavior of L_f can then be a predictor of soot formation in diesel engines. It has been suggested that the premixing of fuel and air upstream of the L_f has a significant effect on the formation of soot in the jet. The larger the L_f, the more air is entrained into the jet upstream of L_f. As the ratio of air entrainment rate to fuel mass flow rate increases, the less soot is formed [1,2]. Experiments have shown that changes in L_f caused by changes in ambient conditions and injection pressure affect the fuel-air mixture at the lift-off height [3]. In this work, a computational model will be employed to explore the relationship between soot formation and L_f.

Table 1 lists a set of measured conditions which will be considered in this work. Measurements were made in a constant-volume chamber (www.sandia.gov/ecn/). The parameters d_{noz}, P_{inj}, P_{amb}, T_{amb}, $\rho_{amb,\ and}$ $O_{2\ \%}$ represent the nominal injector orifice diameter, the injection pressure, the pressure in the chamber, the chamber temperature, the chamber density, and the percentage of oxygen in the chamber, respectively. The structure of vaporizing diesel sprays in conventional diesel engines under high pressure and high temperature conditions has been shown to be momentum-controlled and it can be well-approximated using vapor jets with the same mass and momentum flow rates as the liquid spray [4-7]. In Table 1, d_{gas} is the equivalent diameter of an injector that injects the vapor. Bajaj *et al.* [4] employed the same computational model that will be employed in this work and showed that lift-off heights agree within 25% and ignition delays within 30% of measured values. The measured and computed values are listed in Table 2. The normalized lift-off height L_f^* in Table 2 will be explained later. The present work is an extension of the work of Bajaj *et al.* and computes the soot and NO in the same 9 jets. In this paper only the soot results will be presented. The next section will discuss the computational model employed. Results and discussion will follow. The paper will close with summary and conclusions.

Table 1. Computed conditions

Case	d_{noz} (mm)	d_{gas} (mm)	P_{inj} (MPa)	P_{amb} (bar)	T_{amb} (K)	ρ_{amb} (kg/m^3)	O_2%
1	0.1	0.199	150	42.66	1000	14.8	21
2	0.1	0.199	60	42.66	1000	14.8	21
3	0.1	0.1745	150	55.45	1300	14.8	21
4	0.1	0.2097	150	38.39	900	14.8	21
5	0.1	0.199	150	43.02	1000	14.8	15
6	0.1	0.199	150	43.2	1000	14.8	12
7	0.1	0.199	150	43.45	1000	14.8	8
8	0.18	0.3858	140	42.66	1000	14.8	21
9	0.1	0.1397	150	86.47	1000	30.0	15

Table 2. Computed and measured ignition delay and lift-off height

Case	Ignition Delay (ms)		Lift-off Height (L_f)		
	Measured	Computed	Measured (mm)	Computed (mm)	Normalized (L_f*)
1	0.53	0.542	17.00	18.50	30.57
2	--	0.615	13.50	15.05	24.87
3	0.26	0.209	7.70	8.05	13.43
4	0.79	0.89	25.50	23.30	38.51
5	0.73	0.56	23.20	22.90	37.84
6	0.947	1.225	29.20	27.30	45.11
7	1.52	2.17	42.30	52.88	87.37
8	0.57	0.65	23.97	25.80	21.99
9	0.38	0.175	11.90	12.00	28.24

* Corresponding author:
Email: myen@purdue.edu

2. Computational Model

The REC code employed by Bajaj *et al.* [4] is used in this work. Turbulence is modeled using the k-ε model with boundary layers modeled using wall functions. The REC model has been used in computing diesel jets in many prior studies [5,6]. Considering the turbulent diffusion flame as an ensemble of strained laminar flamelets [8], turbulence/chemistry interactions are modeled using the unsteady flamelet progress variable (UFPV) model [4]. In the model, the averaged chemical source terms are determined using the local temperature T, local mixture fraction Z, and local scalar dissipation rate χ. Instantaneous (non-averaged) chemical source terms are tabulated in libraries as a function of mixture fraction Z, stoichiometric scalar dissipation rate χ_{st}, and the stoichiometric progress of reaction variable C_{st}.

The soot is modeled using a kinetic mechanism [9, 10]. In this model, the polycyclic aromatic hydrocarbons (PAHs), from which soot forms, are formed by Hydrogen-Abstraction-Carbon-Addition (HACA). The method of moments is then used to solve for the soot volume fraction and the soot number density [11,12]. When extending the UFPV model to compute soot, the following approach is used: the soot volume fraction and soot number density are tabulated as a function of the same three variables as for the chemical source terms described earlier. However, since soot variables do not reach equilibrium values, unlike temperature and species mass fractions, time is employed as the progress variable for the soot variables.

A 44-species, 185-step reaction mechanism is employed to model n-heptane oxidation [4]. This mechanism is not suitable for the soot kinetics considered in this study. For this purpose, a 160-species, 1995- step reaction mechanism is employed. When using the RANS model, the average scalar dissipation rate is modeled as [13]

$$\tilde{\chi} = C_{\chi} \frac{\varepsilon}{k} \widetilde{Z''^2}, \qquad (1)$$

where C_{χ} is a constant and Z''^2 is the variance of the mixture fraction. The choice of C_{χ} determines the numerical value of the scalar dissipation rate. In particular, the choice will determine the physical distribution of the scalar dissipation rates in the jet. Bajaj *et al.* [4] concluded that the lift-off height was at the location where the ignition scalar dissipation rate matched the local scalar dissipation rate, i.e. the predicted lift-off height will depend on C_{χ}. The two reaction mechanisms employed have different ignition and extinction scalar dissipation rates. Hence, the value of C_{χ} which predicts measured parameters will be different for variables computed employing the two mechanisms. For the L_f and ignition delay predictions using the 44-species, 185 reaction mechanism for n-heptane for C_{χ} was found to be 6.5 [4].This constant is, however, unlikely to be applicable when the 160-species 1995-step mechanism is employed. Independently of this effect, the constants in the variance equation are likely to need adjustment. For the purpose of this work, C_{χ} has been assumed to be an adjustable constant whose value was optimized to give the best (soot distribution) results for the 9 cases considered.

3. Results and Discussion

Figures 1 (a) – (c) show the development of flooded mixture fraction contours at various times after start of injection (ASI) for Case 1 of Table 1 and Figs. 2 (a) – (c) show the development of the corresponding flooded temperature contours [14,4]. At about 0.55 ms, ignition occurs about 3.4 cm downstream of the orifice, near the leading tip of the jet. As described by Bajaj *et al.* [4], an ignition front propagates outwards from the point of ignition toward the stoichiometric surface (Fig. 2 (a)) followed by flame front propagation upstream along the stoichiometric surface (Fig. 2 (b)). Meanwhile the jet penetrates farther into the chamber. The flame that propagates upstream stabilizes at a lift-off height of 1.8 cm where the ignition scalar dissipation rate is equal to the local scalar dissipation rate (Fig. 2 (b)). As the reacting jet continues to develop, the change in lift-off height is negligible (Fig. 2 (c)).

Now we will present the computed results of soot in the jet, starting with the evolution of soot for Case 1 at various times after ignition at the same 3 instants as Fig. 2. Figure 3 shows the soot volume fraction in the jet. Obviously, the selection of the cut-off values for the volume fraction will affect the visual results. For the selected contour values, soot is not noticeable in the first time instant. Subsequently, the soot volume fraction increases with time and the peak value is observed at increasing axial distances as time increases (compare Figs. 3(b) and (c)). This reflects the combined effect of the soot being advected downstream and additional soot being generated in the jet with increasing time. The peak soot concentrations are confined to the center of the jet along the axis near the head vortex of the jet.

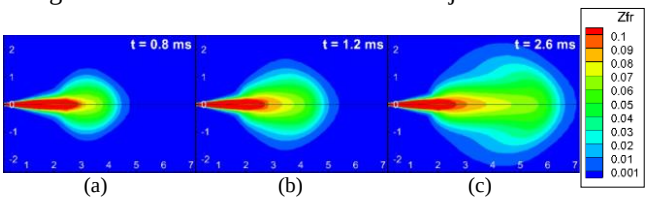

(a) (b) (c)

Figure 1. Development of mixture fraction in jet, Case 1

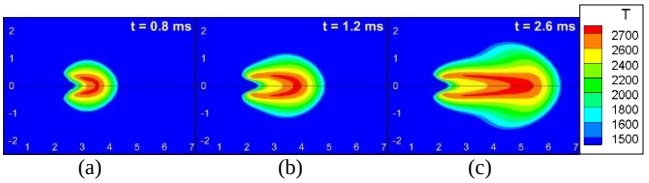

(a) (b) (c)

Figure 2. Flame development in jet, Case 1

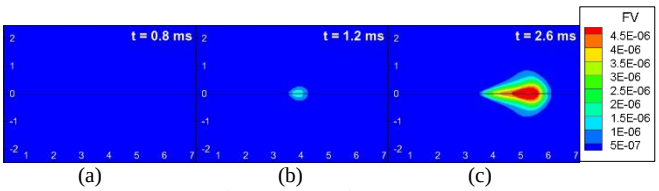

(a) (b) (c)

Figure 3. Development of soot volume fraction in jet, Case 1

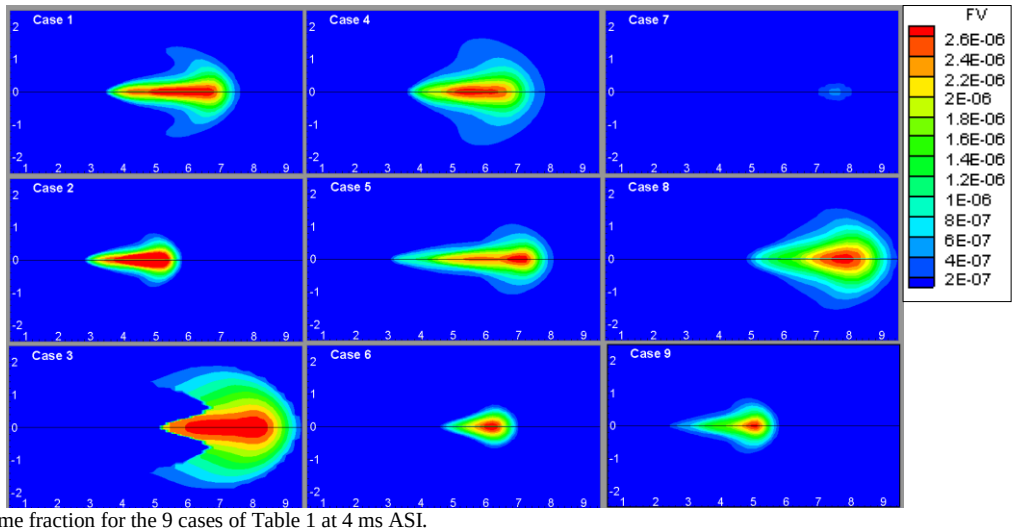

Figure 4. Soot volume fraction for the 9 cases of Table 1 at 4 ms ASI.

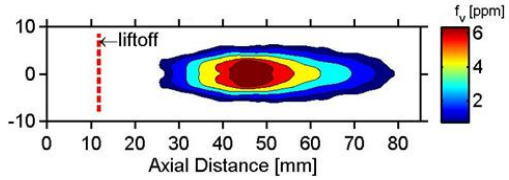

Figure 5. Quasi-steady soot volume fraction distribution of Case 1 (www.sandia.gov/ecn/).

Figure 4 shows the soot distribution for the 9 cases of Table 1 at 4 ms ASI. Figure 5 shows the measured soot volume fraction of Case 1 in the quasi-steady part of the jet. These results are obtained by combining time averaged line-of-extinction data and soot profile LII imaging. Similar results are available for Cases 5, 6, 7, and 9 (www.sandia.gov/ecn/). The time averaging can, of course, be carried out only in the quasi-steady part of the jet. The computed results are shown at 4 ms. The part of the computed jet upstream of the head vortex can be assumed to be at quasi-steady state. In this region, there is qualitative agreement of the measured and computed results in terms of location of peak values and distribution. In fact, there is quantitative agreement within a factor of about three. Table 3 shows the mass of soot m_{soot} in the chamber at 4 ms ASI for the 9 cases. Also shown in Table 3 is m_{soot}* which are values of soot which have been normalized by the total mass of fuel injected during 4 ms.

Next, the correlation of the m_{soot} with L_f and entrained mass m_e at the L_f will be examined. It seems reasonable to assume that the more the air entrained, the less the amount of soot formed. In particular, it appears reasonable to suggest that the more the air entrained upstream of the lift-off height, the less the amount of soot formed downstream of the L_f [1]. Note that the air entrained downstream of the lift-off height is reacted at the flame front. The rate of entrained mass flow rate $\dot{m}_e$ normalized by the injected mass flow rate $\dot{m}_f$ is given by the following expression [7,14]:

$$\frac{\dot{m}_e}{\dot{m}_f} = \frac{Kx}{d}\left(\frac{\rho_a}{\rho_i}\right)^{0.5}, \qquad (2)$$

where K is a constant, $\dot{m}_e$ is the mass flow rate of entrained air, $\dot{m}_f$ is the mass flow rate of fuel injected, x is the axial distance from the orifice, d is the diameter of the nozzle, ρ_a is the density of ambient chamber air, and ρ_i is the density of the injected fuel. In fact, the combination of variables $(1/d)(\rho_a / \rho_i)^{0.5}$ can be considered to be a normalizing variable for the distance. In Table 2, the normalized values of lift-off heights are shown in the last column where

$$L_f^* = L_f\left(\frac{\rho_a}{\rho_i}\right)^{0.5}\left(\frac{1}{d}\right). \qquad (3)$$

It is useful to compute the ratio of entrained to injected mass flow rate at the lift-off height. Results for reacting and non-reacting jets are given in Table 4 along with the results from Eq. (2) where K is chosen to be 0.32 for quasi-steady jets. Comparing the lower injection pressure Case 2 with its baseline Case 1, Table 2 shows that the L_f* is shorter in Case 2. Although the ignition scalar dissipation rates are the same for both cases, the local scalar dissipation for Case 2 is lower as a result of the lower injection velocity and this results in shorter L_f*. Equation (2) shows that at the same axial distance, $\dot{m}_e/\dot{m}_f$ is the same; but, because the L_f is shorter, the ratio is smaller in Case 2 as shown in Table 3. Comparing the normalized value of soot for Case 2 with Case 1, Case 2 is higher as expected. In Case 3 the ambient temperature has been increased to 1300 K which increases the ignition scalar dissipation rate resulting in decreased lift-off height. This decreases the $\dot{m}_e/\dot{m}_f$ at the lift-off height and increases the normalized soot compared to Case 1. Cases 4-7 follow the same argument as Case 3 where a decrease in ignition scalar dissipation rate as a result of lower temperature in Case 4 and progressively lower oxygen concentrations in Cases 5-7 increases the L_f* and therefore increases the $\dot{m}_e/\dot{m}_f$, decreasing normalized soot.

Case 8 is an interesting one because the nozzle diameter is 1.8 times greater compared to Case 1. The ignition scalar dissipation rates of Case 1 and Case 8 are equal. The results suggest that the increase in diameter increases the local scalar dissipation rate and therefore increases the L_f. When normalized, however, L_f* is shorter than Case 1 as seen in Table 2. Equation (2) supports this by showing that the effect of the

increase in diameter results in $\dot{m}_e/\dot{m}_f$ being less than that of Case 1, increasing normalized soot.

Table 3. Computed and calculated $\dot{m}_e/\dot{m}_i$ at lift-off height with actual and normalized mass of soot at 4 ms ASI

CASE	$\dot{m}_e/\dot{m}_i$			m_{soot} (g)	m_{soot} *
	Computed		Calculated		
	Reacting	Non- React	Eq. (11)		
1	10.56	9.81	9.78	6.01E-08	2.23E-05
2	9.18	8.24	7.96	5.51E-08	3.24E-05
3	4.13	3.96	4.30	9.63E-08	3.57E-05
4	14.89	14.04	8.89	3.81E-08	1.41E-05
5	14.40	12.78	12.11	1.43E-08	5.73E-06
6	16.24	15.48	14.43	3.22E-09	1.29E-06
7	29.19	30.48	27.96	1.35E-14	5.41E-12
8	7.33	6.77	7.04	3.62E-07	3.96E-05
9	7.08	8.89	9.03	1.26E-08	4.66E-06

When the chamber density increases in Case 9, the ignition scalar dissipation rate increases. Note that the oxygen content of Case 9 is 15% and the results must be compared with Case 5. Increasing the ignition scalar dissipation rate allows the flame to travel farther upstream before the flame stabilizes. L_f* for Case 9 is higher than the L_f* of Case 5 which explains the decrease in normalized soot.

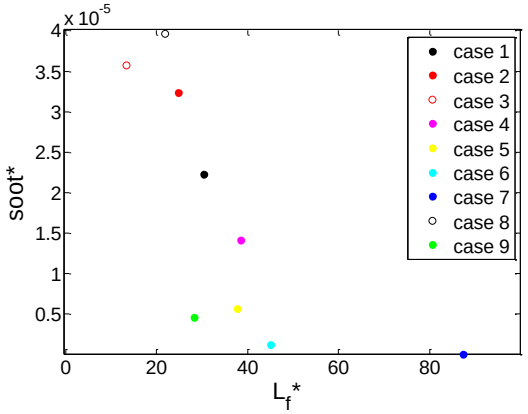

Figure 6. Normalized soot mass vs. normalized lift-off height at 4 ms

Figure 6 shows the normalized mass of soot as a function of the normalized lift-off height. Recall that the soot mass is normalized by mass of fuel injected, and the lift-off height by the appropriate combination of nozzle diameter, injected density, and chamber density shown in Eq. (3). We can see clearly that the soot* decreases for increasing L_f*. There are a couple of outliers: Cases 3 and 9, where the soot* is lower than expected for the L_f* given. The correlation between mass of soot and lift-off height is based on the effect of the mixing on soot *formation*. The net soot mass in the jet is, however, controlled by both *formation* and *oxidation*. Of course, during fuel injection, the influence of oxidation is generally less important than of formation. Nevertheless, oxidation will have an effect. It is possible that in Cases 3 and 9 the oxidation is more dominant, as a result of higher temperature and density, compared to the other 7 cases. As a result, the actual soot is lower than what it would have been if formation alone were controlling the mass of soot. Note that in Case 7, the mass of soot is negligible and, hence, its position with respect to the trend curve is not important.

4. Summary and Conclusions

The earlier work of Bajaj *et al.* [4] on modeling flame lift-off in diesel jets is extended to model soot in the lifted jets within the framework of the unsteady flamelet progress variable (UFPV) model employed by Bajaj *et al.* The computed distribution of soot in the jet is found to be qualitatively similar to measured distributions. When the soot mass and lift-off heights are appropriately normalized, the results show that the normalized mass of soot correlates well with the normalized lift-off height, i.e. higher lift-off height results in lower soot mass. It is shown that this correlation arises from changes in entrained mass upstream of the lift-off height. These results and conclusions are applicable only during the period of injection. The soot in the exhaust of an engine is dependent on oxidation characteristics of soot once injection ends, i.e. during the expansion stroke. In fact, the oxidation effects may be the dominant factor. Further extension of this work is required to understand the dependence of *exhaust* soot emissions on lift-off.

5. Acknowledgments

The authors are grateful to Caterpillar, Inc. for providing the funding for this work.

6. References

[1] D.L. Siebers, B.S. Higgins, SAE 2001-01-0530 (2001).
[2] L.M. Pickett, D.L. Siebers, SAE 2003-01-3080 (2003).
[3] L.M. Pickett, D. L. Siebers, Combust. Flame 138 (2004) 114-135.
[4] C. Bajaj, M. Ameen, J. Abraham, Combust. Sci. and Technol. 185 (2013) 454-472.
[5] V. Iyer, J. Abraham, Combust. Sci. and Technol. 130 (1997) 315-334.
[6] J. Abraham, L. Pickett, Atomization Sprays 20 (2010) 241–250.
[7] C. Bajaj, J. Abraham, L. Pickett, Atomization Sprays 21 (2011) 411–426.
[8] N. Peters, Prog. Energy Combust. Sci. 10 (1984) 319-339.
[9] M. Frenklach, H. Wang, Proc. Combust. Inst. 23 (1991) 1559-1566.
[10]J. Appel, H. Bockhorn, M. Frenklach, Combust. Flame 112 (2000) 122-136.
[11]M. Frenklach, S.J. Harris, J. Colloid Interface Sci., 118 (1987) 252-261.
[12]V. Gopalakrishnan, J. Abraham, Combust. Sci. Technol. 17 (2004) 603-641.
[13] W.P. Jones, J.H. Whitelaw, Combust. Flame, 48 (1982) 1-26.
[14] J. Abraham, Numer. Heat Transf., 30 (1996) 347–364.